

Smectic Phases

Polar Order in a Fluid Like Ferroelectric with a Tilted Lamellar Structure – Observation of a Polar Smectic C (SmC_P) Phase

Jordan Hobbs,* Calum J. Gibb, Damian Pocięcha, Jadwiga Szydłowska, Ewa Górecka, and Richard J. Mandle

Abstract: The discovery of fluid states of matter with spontaneous bulk polar order is appreciated as a major discovery in the fields of soft matter and liquid crystals. Typically, this manifests as polar order superimposed atop conventional phase structures and is thus far limited to orthogonal phase types. Here we report a family of materials which exhibit a previously unseen state of matter which we conclude is a polar smectic C phase, and so we term it SmC_P. The spontaneous polarisation of the SmC_P phase is over two orders of magnitude larger than that found in conventional ferroelectric SmC phase of chiral materials used in some LCD devices. Fully atomistic molecular dynamics simulations faithfully and spontaneously reproduce the proposed structure and associated bulk properties; comparison of experimental and simulated X-ray scattering patterns shows excellent agreement. The materials disclosed here have significantly smaller dipole moments than typical polar liquid crystals such as RM734 which suggests the role of molecular electrical polarity in generating polar order is perhaps overstated, a view supported by consideration of other molecular systems.

Introduction

Since its discovery in 2017^[1–3] and subsequent confirmation of discovery in 2020,^[4–7] the ferroelectric nematic phase (N_F)

has been shown to have a rich variety of properties such as non-linear optical properties,^[8] extreme interfacial instabilities,^[9] bulk photovoltaic effect,^[10] extreme polarisation screening,^[11] and piezoelectric properties^[12] to name a few, where all these properties have their origins in the large longitudinal spontaneous polarisation ($> 4 \mu\text{C cm}^{-2}$) caused by the lack of inversion symmetry of the N_F phase (Figure 1a).^[13,14]

Longitudinal polarisation of liquid crystalline materials is not isolated to the nematic phase and more exotic phase structures have been discovered^[14] such as the ferroelectric smectic A (SmA_F) phase^[15–17] where the polarisation vector is parallel to the layer normal. An antiferroelectric smectic A (SmA_{AF}) phase has also recently been discovered^[18,19] although the exact nature of the anti-ferroelectric ordering within those systems is not yet clear. Perhaps even more interesting is the recent discovery of longitudinally polar LC phases which spontaneously break chiral symmetry, presumably due to the high spontaneous polarisation, such as the so-called twist bend ferroelectric nematic phase (N_{TBF})^[20,21] and the heliconical polar smectic C phase (SmC^H_P).^[18] It has recently been suggested that since these LC phases with longitudinal polarity are proper ferroelectrics (i.e. caused by dipolar interactions rather than steric interactions) polar order could effectively be superimposed over the orientation and positional order of the underlying LC phase.^[19] A logical progression of this idea would suggest the existence of longitudinally polar variants of many of the known non-polar LC phases.

In apolar liquid crystals, it is widely understood that fluorination of the rigid core unit generally suppresses smectic phase formation^[22,23] and it was shown that removal of adjunct fluorine atoms from the archetypal ferroelectric nematogen **DIO**^[3] leads to the formation of a SmA_F phase.^[16] The dioxane moiety found in **DIO** is also known to suppress smectic phase formation.^[24] Most studies into novel ferroelectric nematogens and smectogens have focused on increasing molecular fluorination,^[25] here we show that exchange of the dioxane ring for a phenyl moiety coupled with the removal of all adjunct fluorine atoms (the **PPZGU-n-F** series, Figure 1b) further promotes the formation of smectic phases with bulk polar order, leading to the observation of a both a SmA_F phase and a polar, titled smectic phase (Figure 1a [right]).

[*] Dr. J. Hobbs, Dr. R. J. Mandle
 School of Physics and Astronomy
 University of Leeds
 Leeds, UK, LS2 9JT
 E-mail: j.l.hobbs@leeds.ac.uk

Dr. C. J. Gibb, Dr. R. J. Mandle
 School of Chemistry
 University of Leeds
 Leeds, UK, LS2 9JT

Dr. D. Pocięcha, Dr. J. Szydłowska, Prof. E. Górecka
 Faculty of Chemistry
 University of Warsaw
 ul. Zwirki i Wigury 101, 02-089, Warsaw, Poland

© 2024 The Author(s). Angewandte Chemie International Edition published by Wiley-VCH GmbH. This is an open access article under the terms of the Creative Commons Attribution License, which permits use, distribution and reproduction in any medium, provided the original work is properly cited.

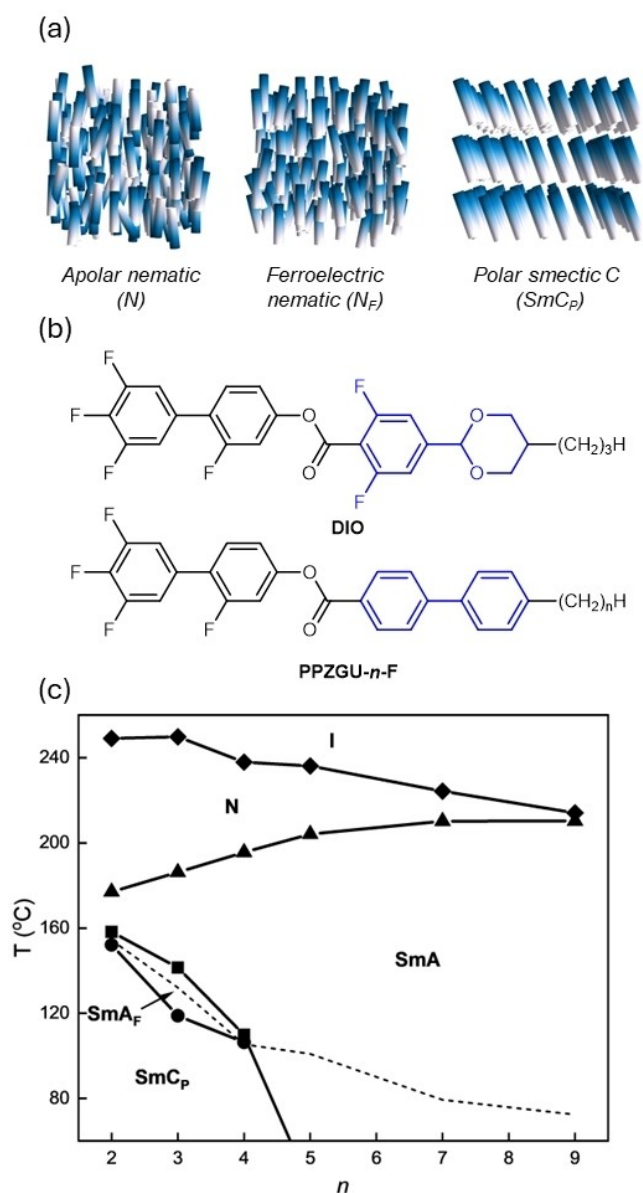


Figure 1. Schematic representations of the (a) conventional N, N_F and SmC_P mesophases; (b) the chemical structure of the archetypal N_F materials DIO^[3] and the general structure of the PPZGU-*n*-F materials reported in this work. The difference in molecular structure between DIO and PPZGU-*n*-F are highlighted in blue; (c) phase diagram showing the evolution of phase behavior on increasing alkyl chain length (*n*) for the PPZGU-*n*-F materials. Melting points are denoted by the dotted line.

Results and Discussion

Transition temperatures of the PPZGU-*n*-F materials are given in Figure 1c (tabulated data in the ESI; Table S1) and were determined by differential scanning calorimetry (DSC), with phase assignments made by polarised optical microscopy (POM), assisted by X-ray scattering and current response studies (*vide infra*). For the sake of brevity, we will focus our discussion on the homologue with *n* = 3 as a representative example of the phase behaviour of the

PPZGU-*n*-F series with supplementary results for the other materials found in the ESI.

PPZGU-3-F shows apolar nematic (N) and smectic A (SmA) phases (as do all other homologues), identified using POM and X-ray scattering, as well as two further LC phases observed on further cooling. Confinement between untreated glass slides typically resulted in homeotropic alignment for the N and SmA phases while for the two lower temperature phases, uncharacteristic textures were observed. However, confinement in cells treated for homeotropic alignment resulted instead in degenerate planar alignment (Figure S1). In X-ray scattering experiments, both the N and SmA phases show diffuse scattering at wide-angles, indicating liquid-like order in direction perpendicular to the director. The lamellar structure of the SmA phase leads to the Bragg scattering of X-rays at small angles (whereas the nematic has only diffuse scattering), yielding a layer spacing (*d*) of 25.0 Å (Figure 2a) which is largely temperature independent across the entire phase range. To obtain the layer spacing (*d*) as a ratio of molecular length (*L*) we performed molecular geometry optimisation at the B3LYP-GD3BJ/cc-pVTZ level; using this value affords a ratio of ~1.07, indicating a near monolayer arrangement of the molecules within the smectic layers. Current response measurements demonstrate that the N and SmA phases are apolar, with only small ionic and dielectric contributions being detected. Notably however, below 150 °C (still in the SmA phase), a single broad peak centred around polarity reversal is observed in the SmA phase (Figure S4), presumably the result of pre-translational field induced polarisation.

For the three shortest homologues studied (*n* = 2–4), two further phases are observed upon cooling the apolar SmA phase. X-ray scattering shows that both phases have a liquid-like smectic structure, with diffuse scattering at wide angles and sharp Bragg scattering in the small angle region (Figure 2b). Subsequent experiments, detailed below, identify these phases as SmA_F and a newly discovered tilted phase with bulk polar order. At the transition from the SmA into the SmA_F phase (i.e. the onset of polar order signified by a single peak in the current response, Figure 2c) there is a slight contraction of layer spacing while the low-angle peak remains a single lobe. From quantum chemical calculations at the B3LYP-GD3BJ/cc-pVTZ level of DFT PPZGU-3-F is shown to have an angle of 10.7° between the dipole vector and the long molecular axis (Figure 2d, Table S2). A SmA_F phase comprised of such molecules could result in a layered structure where the dipoles are aligned normal to the layer planes with the long molecular axes inclined at an angle relative to the layer normal. For this phase to be uniaxial, and be SmA type rather than SmC, the inclined molecules would need to be distributed around a cone and such a structure would be analogous to a de Vries SmA structure.^[25] Such a structure would explain the reduction in layer spacing (Figure 2a) in the SmA_F phase. While the proposed tilt angle here is less than the 10.7° suggested by the DFT calculations this is perhaps not so surprising as the DFT calculations are of a single gas phase molecule and are not completely representative of a molecule in the con-

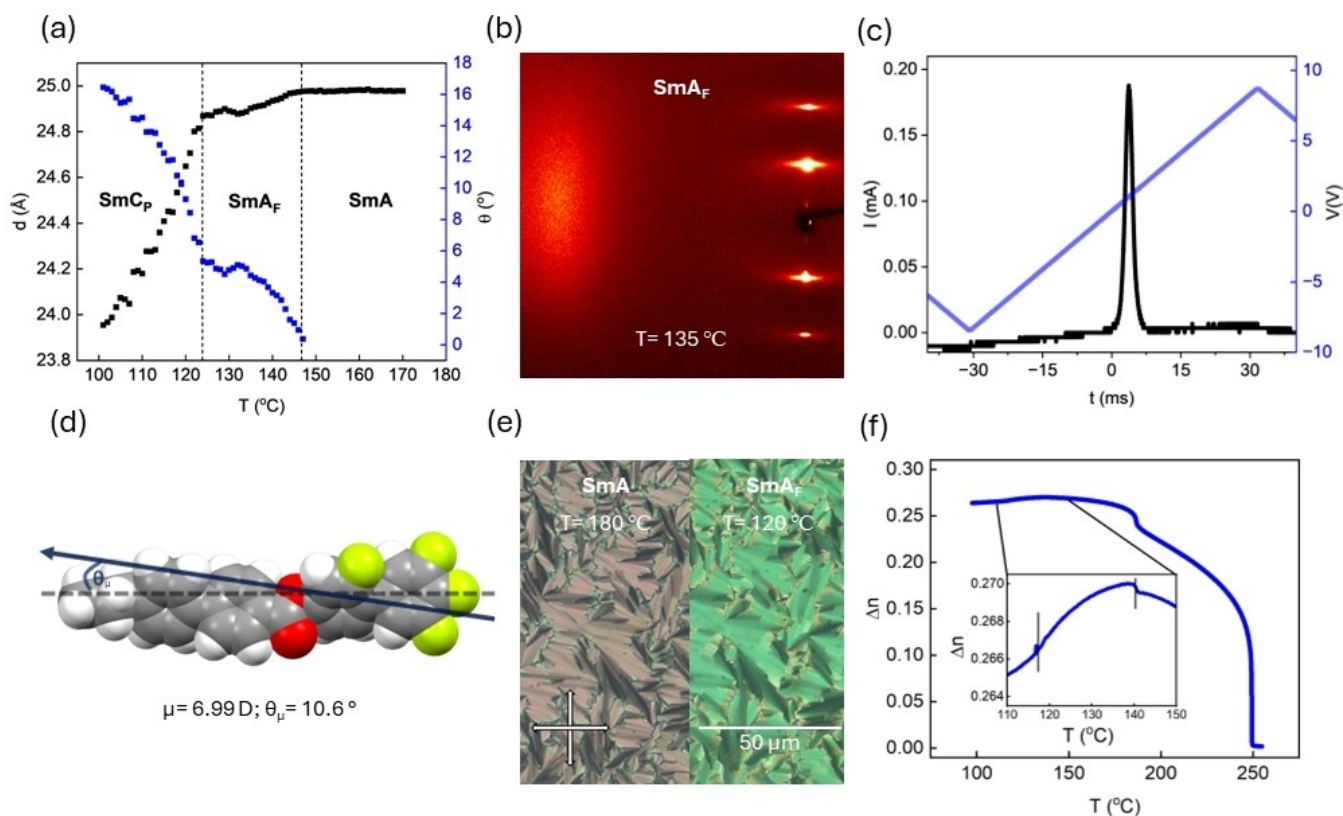


Figure 2. (a) Temperature dependence of the layer spacing for **PPZGU-3-F** in the SmA, SmA_F and SmC_p phases, Tilt angle for the SmA_F phase is the angle between layer normal and long molecular axis assuming a conical De Vries like molecular distribution as described in the text while for the SmC_p phase it is a general bulk uniform tilt angle. (b) 2D x-ray diffraction pattern for **PPZGU-3-F** in the SmA_F phase ($T = 135\text{ }^{\circ}\text{C}$), (c) current response trace measured at 8 Hz in the SmA_F phase ($T = 136\text{ }^{\circ}\text{C}$), (d) the energy minimised geometry of **PPZGU-3-F** calculated at the B3LYP-GD3B/cc-pVTZ level of DFT. The long molecular axis is marked by the hashed line with the direction of the longitudinal molecular dipole moment (inclined at an angle relative to the long molecular axis) marked by the arrow ($\mu = 6.99\text{ D}$; $\theta_{\mu} = 10.6\text{ }^{\circ}$), (e) POM micrographs of the SmA ($T = 180\text{ }^{\circ}\text{C}$) [left] and SmA_F [right] ($T = 120\text{ }^{\circ}\text{C}$) phases. **PPZGU-3-F** samples are confined in thin cells treated for a homeotropic anchoring condition, and (f) the temperature dependence of the optical birefringence, $T(\Delta n)$, for **PPZGU-3-F** measured using green light, $\lambda = 532\text{ nm}$ in a $1.7\text{ }\mu\text{m}$ cell treated for planar alignment.

densified LC phases. There would also be further contributions to the tilt angle from the polar and orientational order of the phase. We also note for the Bragg scattering associated with the lamellar structure up to 6th order harmonic can be observed, although this limit is due to the Q limits of the detector rather than because we could not observe the 7th order fringe (Figure S3). Generally, for a SmA phase the layers are diffuse and more of a density modulation rather than strict layers. However, the observation here of several harmonics of the diffraction signal due to layered structure means that the density modulation along the layer normal is strongly non-sinusoidal giving rather sharp boundaries between the high- and low-density regions. The long-range correlation of the layers may be due to a lack of layer undulations as these would lead to areas of bound charge due to splay of the polarisation in those regions.^[26]

For the SmA_F phase the current response shows that the pretransition peak observed for the SmA phase moves to higher voltage, indicating the increased threshold for switching (Figure 2c). This increase is possibly due to the increased

cost of rotating the smectic layers along with the polarisation where the maximum value of polarisation in the SmA_F phase is $\sim 3.0\text{ }\mu\text{C cm}^{-2}$ (Figure S5). The non-centrosymmetric structure of the SmA_F phase is further affirmed by second harmonic generation (SHG) microscopy (Figure S6), where the presence of an SHG signal without biasing electric field confirms the polar ground state of the SmA_F phase.

Optically, the SmA_F phase retains the fan texture observed in the preceding apolar SmA phase, however the texture now contains regions of rapidly changing retardance (Figure S1). These defects generally form out of fan domain boundaries of the SmA phase, indicative of the rotation of the vertical director at regions where the sign of the polarization switches without forming a line defect (Figure 2e). Such observations are suggested to be characteristic of the SmA_F phase.^[18,19] We propose that the texture observed in these materials is somewhat paramorphic, as it has been suggested that polar ordering prohibits the formation of Dupin cyclides responsible for the fan and focal conic textures in the apolar SmA phase.^[16] In anti-parallel rubbed planar cells, a clear transition can only be

observed when comparing the dark states of both phases via comparison of the defects which form around the spacer beads (Figure S7). In general, when anti-parallel rubbed planar cells are used to confine the N_F phase, π -twist domains can form, due to polar surface interactions^[28] and to minimize the bulk polarisation of the system.^[29] Such domains are not observed within the SmA_F phases studied here, consistent for when the phase is formed from a preceding N_F phase.^[15] Optical birefringence (Δn) was measured by cooling throughout the whole LC phase range (Figure 2f). In the N phase a power law temperature dependence was observed, with a small jump in Δn on transition to the SmA phase. Another slight step (~ 0.01) was detected for the SmA - SmA_F transition before a slight decrease is observed throughout the SmA_F phase. Although this could be due to a slight reduction in alignment quality, POM images of the dark state of these materials does not imply any change in the quality of alignment and we instead suggest that this is further evidence for the adoption of a de Vries like molecular orientation.

Further cooling of the SmA_F phase for homologues with $n < 5$ sees a transition to a final liquid-like smectic phase. Here, the Bragg scattering of the SmA_F is retained though a continuous decrease in the layer spacing, indicating a tilting of the molecules away from the layer normal (i.e. a SmC -like phase), is now observed. For all the homologues studied, the tilt does not saturate at the point of crystallisation ($\sim 16^\circ$ at 100°C for **PPZGU-3-F**; Figure 2a). Within a cell treated for homeotropic anchoring, the fan-like texture of the preceding SmA_F splits into small domains, forming a broken fan-like texture (Figure 3a), where each domain corresponds to different tilt direction. The formation of these domains disrupts the alignment of the sample when confined within cells treated for planar anchoring, resulting in the complete loss of any extinction condition upon rotating the cell with respect to the polarisers' direction (Figure S8d). The lack of alignment in planar cells prohibits the reliable measurement of birefringence via the technique used here. Measurements of the current response reveal that the polarity of the SmA_F phase is retained (Figure 3b), with the position of the main peak observed in the preceding phase moving backwards towards lower voltage indicating a decreased elastic cost of bulk polarisation reversal, with the P_S saturating at a value of $3.3 \mu\text{C cm}^{-2}$ a value two orders of magnitude larger than for the conventional chiral smectic C (SmC^*) phase.^[30] However, a second peak of a smaller magnitude to the main signal, emerges in the current response upon entering the new phase just before applied voltage polarity reversal. Such a current response would not result in a truly "ferroelectric" hysteresis loop, owing to the observation of multiple peaks. This peak is possibly due to some ionic effect induced by the emergence of tilt domains, or it could be associated with tilt removal, analogous to a mechanism suggested for the recently discovered helical polar SmC phase,^[18] though we note no evidence for helix formation is observed for the materials presented here. The polar nature of the lowest temperature smectic phase is further confirmed by SHG microscopy (Figure S6) though whether the phase is "ferroelectric" or some other type of

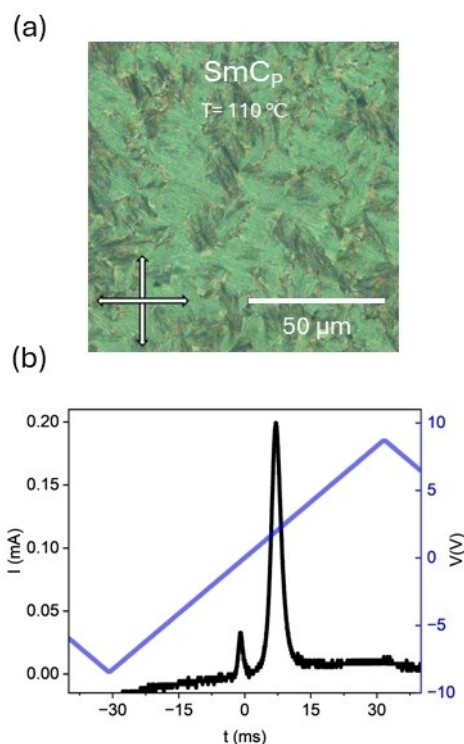


Figure 3. (a) POM micrographs of the broken fan texture of the SmC_p ($T = 110^\circ\text{C}$) phase observed for **PPZGU-3-F**. The image is taken of a sample confined within a thin cell treated for homeotropic anchoring; (b) current response trace measured at 8 Hz in the SmC_p phase ($T = 104^\circ\text{C}$) showing the emergence of a second smaller peak at longer time scales.

polar ordering is not yet clear from performed measurements and thus we term this phase the polar smectic C phase (SmC_p).

We sought to validate the structure proposed above using fully atomistic molecular dynamics simulations, during which (and under certain conditions) the SmC_p phase forms spontaneously. Our simulations initially begin from either an isotropic or polar nematic configuration, which evolve into apolar and polar phases, respectively. Gratifyingly, both apolar and polar initial configurations yield the correct phase sequences, with bulk properties and transition temperatures in reasonable agreement with experiment. Simulations commencing from an isotropic state remain isotropic at and above 252°C , while the simulation at 227°C evolves into a nematic phase ($\langle P2 \rangle = 0.61 \pm 0.04$) (Figure S8). At and below 202°C , the simulations evolve into an SmA phase with layer spacing of $2.4 \pm 0.1 \text{ nm}$ (Figure S10). At no point does the apolar simulation evolve into a tilted smectic phase.

Simulations commencing from a polar nematic configuration evolve into an isotropic state (at and above 252°C) and slowly transform to a non-polar N phase on cooling (227°C). The orientational order parameter is retained, while the polar order parameter tends to zero over the first 140 ns (Figure S9). At and below 202°C , a polar SmA phase spontaneously forms with $\langle P1 \rangle = 0.94 \pm 0.01$ and $\langle P2 \rangle >$

$= 0.78 \pm 0.02$. The simulated SmA phase has a layer spacing of 2.3 (± 0.1) nm and spontaneous polarisation value of 2.5 (± 0.02) $\mu\text{C cm}^{-2}$, both of which are in harmony with the values obtained by experiment. Crucially, at and below 202 °C, the molecules spontaneously tilt away from the layer normal, resulting in the formation of a tilted smectic phase with bulk polar order, analogous to the SmC_p phase proposed based on experimental observations (Figure 4c). The *in-silico* SmC_p phase has a layer spacing of 2.2 ± 0.1 nm and a tilt angle of 25 ± 3 °, which are in reasonable agreement with experimentally obtained values (2.4 nm and 16 °, respectively). The SmC_p phase has a near

saturated polar order parameter ($\langle P_1 \rangle = 0.90 \pm 0.04$) and orientational order consistent with a fluid smectic phase ($\langle P_2 \rangle = 0.78 \pm 0.06$).

We used the MD trajectory to simulate a 2D SAXS pattern of the SmC_p phase by mapping the atomic electron density onto a 3D grid and transforming into the structure factor via Fourier transform (see ESI). The simulated 2D SAXS pattern closely matches that obtained experimentally (Figure 4a and 4b), with diffuse wide-angle scattering and multiple high intensity low-angle peaks. Periodic noise in the simulated SAXS background arises from the Fourier Transform procedure. Additionally, the system size (1000 molecules) and limited simulation duration (500 ns) conspire to introduce further artifacts, such as finite-size effects and incomplete sampling of long-range correlations. The qualitative agreement between experimental/simulated 2D SAXS patterns, along with the ability of the MD simulation to accurately recreate experimentally measured properties, gives a high degree of confidence in our model of the SmC_p phase.

Although the interpretation of the dielectrics of longitudinally polar liquid crystal phases is not yet fully understood,^[31–35] we elected to probe the dynamic properties of **PPZGU-3-F** by dielectric spectroscopy in the SmA, SmA_F and SmC_p phases. Complex permittivity data was obtained for samples in 10 μm thick cells with untreated gold electrodes (Figure S12a, S12b), with the caveat that the dielectric strengths and relaxation times of any relaxation processes will be dependent on the sample thickness, orientation, and anchoring behaviour. Figure 5a contains representative dielectric loss data for **PPZGU-3-F** for the SmA_F and SmC_p phases (details of fitting given in ESI with example of the deconvoluted fits, and Figures 5b and 5c show the relaxation times and dielectric strength for the processes observed through the SmA, SmA_F and SmC_p phases (α fitting parameter is shown in Figure S12c). In the SmA phase, only a single dielectric process was observed (P1). Power laws were used to account for a low frequency conductivity flank and for any processes observed at time-scales faster than the frequency window. P1 shows a super-Arrhenius, Vogel-Fulcher-Tammann (VFT) dependence of its relaxation times typical of cooperative processes with asymptotic behaviour at the transition to the SmA_F phase. We suggest that this process is related to rotations around the short molecular axis which become frozen out at the SmA-SmA_F transitions due to the emergence of polar order. Due to the formation of small ferroelectric clusters in the SmA phase, indicated by the strong pre-transitional induced polarisation (Figure S5), the dielectric strength of P1 also shows significant growth approaching the transition to the polar phase (~ 100 at the SmA-SmA_F transition), behaviour analogous to the N_F phase.^[36]

In the SmA_F phase two processes are observed. A weak mode (P2) appears with a timescale of roughly 10^{-5} s and very large distribution parameter. The timescales and dielectric strength of this process are essentially temperature independent in the SmA_F phase, only consistently moving to longer timescales and steeply increasing in strength (circa 2 orders of magnitude) upon approach to the SmC_p phase.

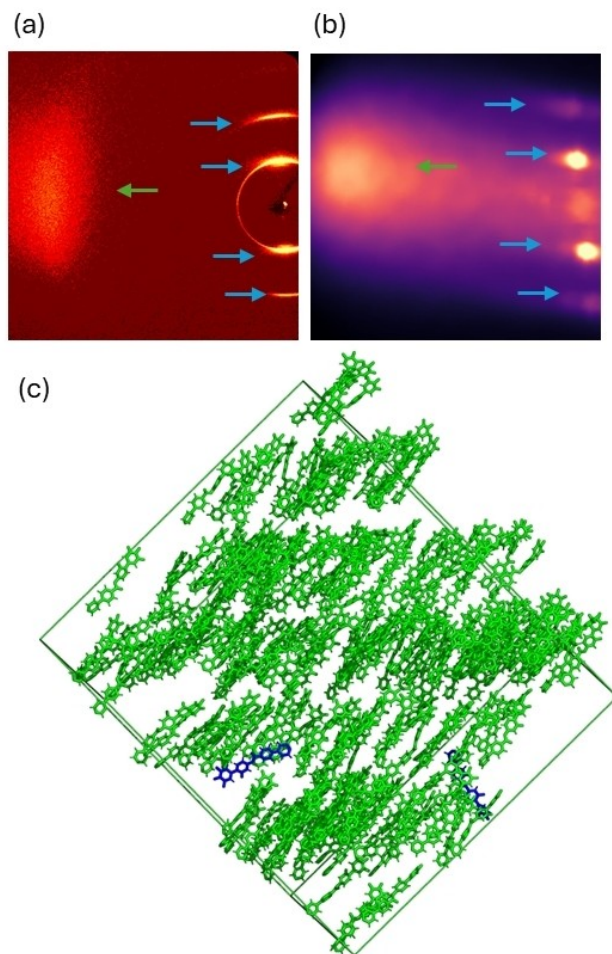


Figure 4. (a) an experimental 2D x-ray diffraction pattern for **PPZGU-3-F** in the SmC_p phase ($T = 115$ °C); (b) simulated 2D SAXS pattern of the SmC_p phase of **PPZGU-3-F** at 127 °C based on the MD trajectory showing good agreement with the data obtained by experiment; and (c) Instantaneous configuration of the polar smectic C phase for the $n = 3$ homologue formed spontaneously from the initial polar configuration at the same temperature ($\langle P_2 \rangle = 0.78 \pm 0.06$). The snapshot is color-coded green/blue to show molecules whose dipole is parallel or antiparallel with the director, respectively ($\langle P_1 \rangle = 0.90 \pm 0.04$). The hydrocarbon chains are omitted from the rendering to aid visualisation of the layer structure (layer spacing = 2.3 ± 0.1 nm; tilt angle = 25 ± 3 °). The calculated spontaneous polarisation (P_s) is 3.2 ± 0.01 $\mu\text{C cm}^{-2}$. Only 400 molecules (out of 1000) are shown, to aid visualisation.

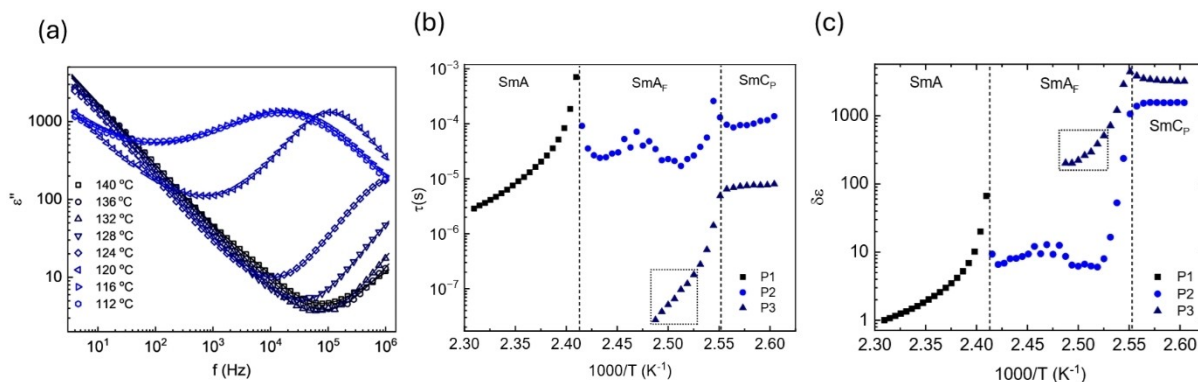


Figure 5. (a) Representative dielectric loss spectra for **PPZGU-3-F** in the SmA_F and SmC_P phases. Line through the data corresponds to the fits obtained; (b) Arrhenius plot of relaxation times; and (c) dielectric strength parameter obtained. The dashed box area in each plot corresponds to areas where P3 was at the edge and outside the fitting window reducing the fit quality in that region.

The main relaxation mode observed in the SmA_F phase (P3) is moving into the frequency window from shorter time-scales. As the SmC_P phase is approached, P3 steeply increases in strength and slows down (Figure 5b, c). In the SmC_P phase, the strong P3 dominates dielectric response, it is only weakly temperature dependent for both its timescale and dielectric strength (in fitting procedure the much weaker P2 mode was also used to ensure the continuous evolution of the modes). We suggest that P3 that starts to develop in SmA_F phase is related to tilt fluctuations, which increase in strength as the molecular motions become more cooperative near phase transition to tilted SmC_P phase. In SmC_P phase the relaxation process P3 is attributed to collective rotation of molecules, and thus polarization, on the tilt cone.

Ultimately the generation of polar ordering in real-world experimental conditions is principally a product of molecular structure, and while a full structure-property relationship is beyond the scope of this initial communication, some striking trends are immediately apparent. Firstly, considering **DIO**^[3] as a starting point, we see that the removing of fluorine atoms from the molecular structure gives a progressively higher onset temperature for polar ordering (either to N_F, N_X, or SmA_F; Figure 6a).^[16] Similarly, replacement of the dioxane unit of **DIO** with phenyl ring - material **PIO**^[19] - increases the propensity for smectic phase formation (Figure 6b). Further reduction of the molecular polarity, achieved by removing fluorine substituents from **PIO**, yields the **PPZGU-*n*-F** materials reported here (Figure 6b) which dramatically increases the onset temperature of polar ordering. We also note that replacement of the dioxane moiety with a phenyl ring only decreases polar-apolar transition temperature (TP) by 10 °C despite the significant reduction (1-2 D) in dipole moment. These two observations run counter to the view that molecular polarity alone generates bulk polar ordering, evidenced by calculated molecular dipole moments which are given in Figure 6b, and we note that the molecules presented here result in one of the lowest reported molecule dipoles to form an LC phase.^[37] Even further reduction in polarity by removing subsequent fluorine atoms gives non-polar phase types (**PPZPU-**

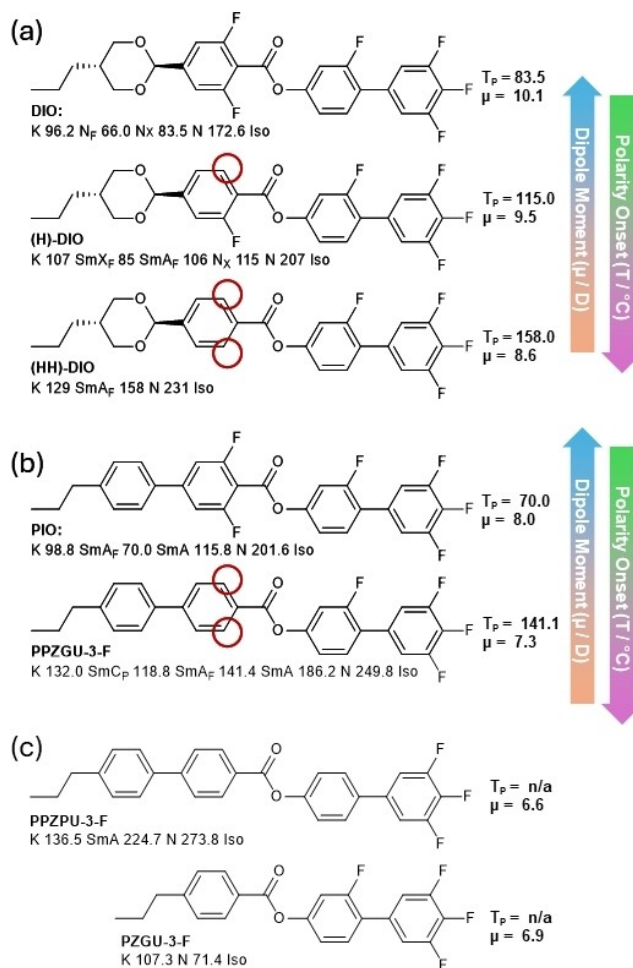


Figure 6. Molecular structures, transition temperatures (°C) and dipole moments (μ ; at the B3LYP-GD3BJ/cc-pVTZ level of DFT) of (a) **DIO**^[3] and similar selected analogues;^[16] (b) **PIO**^[19] and **PPZGU-3-F**, the later from this work; (c) the non-polar derivatives of **PPZGU-3-F** and **PIO**, **PPZPU-3-F** (of this work) and **PZGU-3-F**,^[19] respectively.

3-F; this work, see ESI). We also note the importance of molecular length in arresting head-to-tail flipping, as

- [18] C. J. Gibb, J. Hobbs, D. I. Nikolova, T. Raistrick, S. R. Berrow, A. Mertelj, N. Osterman, N. Sebastián, H. F. Gleeson, R. J. Mandle, *Nat. Commun.* **2024**, *15*, 5845.
- [19] J. Hobbs, C. J. Gibb, R. J. Mandle, *Small Sci.* **2024**, *4*, 2400189.
- [20] J. Karcz, J. Herman, N. Rychłowicz, P. Kula, E. Górecka, J. Szydłowska, P. W. Majewski, D. Pocięcha, *Science* **2024**, *384*, 1096.
- [21] H. Nishikawa, D. Okada, D. Kwaria, A. Nihonyanagi, M. Kuwayama, M. Hoshino, F. Araoka, *Adv. Sci.* **2024**, 2405718. 10.1002/advs.202405718.
- [22] M. Hird, *Chem. Soc. Rev.* **2007**, *36*, 2070.
- [23] G. W. Gray, M. Hird, K. J. Toyne, *Mol. Cryst. Liq. Cryst.* **1991**, *195*, 221.
- [24] R. J. Mandle, C. J. Gibb, J. L. Hobbs, *Liq. Cryst.* **2024**, *51*, 1384.
- [25] R. J. Mandle, *Soft Matter* **2022**, *18*, 5014.
- [26] S. T. Lagerwall, P. Rudquist, F. Giesselmann, *Mol. Cryst. Liq. Cryst.* **2009**, *510*, 1282.
- [27] L. Paik, J. V. Selinger, *arXiv [Cond-Mat.Soft]* **2024**. 10.48550/arXiv.2408.10347.
- [28] X. Chen, E. Korblova, M. A. Glaser, J. E. MacLennan, D. M. Walba, N. A. Clark, *PNAS* **2021**, *118*, e2104092118.
- [29] P. Kumari, B. Basnet, M. O. Lavrentovich, O. D. Lavrentovich, *Science* **2024**, *383*, 1364.
- [30] S. T. Lagerwall, *Handbook of Liquid Crystals* **2014**, pp. 1–258.
- [31] N. A. Clark, X. Chen, J. E. MacLennan, M. A. Glaser, *Phys. Rev. Res.* **2024**, *6*, 13195.
- [32] A. Adaka, M. Rajabi, N. Haputhantrige, S. Sprunt, O. D. Lavrentovich, A. Jákli, *Phys. Rev. Lett.* **2024**, *133*, 38101.
- [33] N. Vaupotič, D. Pocięcha, P. Rybak, J. Matraszek, M. Čepič, J. M. Wolska, E. Gorecka, *Liq. Cryst.* **2023**, *50*, 584.
- [34] V. Matko, E. Gorecka, D. Pocięcha, J. Matraszek, N. Vaupotič, *arXiv [Cond-Mat.Soft]* **2024**. 10.48550/arXiv.2401.16084.
- [35] A. Erkoreka, J. Martinez-Perdiguero, *Phys. Rev. E* **2024**, *110*, L022701.
- [36] S. Brown, E. Cruickshank, J. M. D. Storey, C. T. Imrie, D. Pocięcha, M. Majewska, A. Makal, E. Gorecka, *ChemPhysChem* **2021**, *22*, 2506.
- [37] H. Matsukizono, Y. Sakamoto, Y. Okumura, H. Kikuchi, *J. Phys. Chem. Lett.* **2024**, *15*, 4212.
- [38] C. J. Gibb, R. J. Mandle, *J. Mater. Chem. C Mater.* **2023**, *11*, 16982.
- [39] J. Li, Z. Wang, M. Deng, Y. Zhu, X. Zhang, R. Xia, Y. Song, Y. Hisai, S. Aya, M. Huang, *Giant* **2022**, *11*, 100109.
- [40] E. Cruickshank et al., *ACS Omega* **2023**, *8*, 36562.
- [41] G. J. Strachan, E. Górecka, J. Szydłowska, A. Makal, D. Pocięcha, *arXiv [Cond-Mat.Soft]* **2024**. 10.48550/arXiv.2408.07381.
- [42] H. Kikuchi, H. Nishikawa, H. Matsukizono, S. Iino, T. Sugiyama, T. Ishioka, Y. Okumura, *arXiv [Cond-Mat.Soft]* **2024**. 10.48550/arXiv.2408.09520.

Manuscript received: August 28, 2024

Revised manuscript received: October 16, 2024

Accepted manuscript online: October 30, 2024

Version of record online: November 14, 2024